Acta Materialia 165 (2019) 87–98

Contents lists available at ScienceDirect

Acta Materialia

journal homepage: www.elsevier.com/locate/actamat

Full length article

Deformation compatibility between nanotwinned and recrystallized grains enhances resistance to interface cracking in cyclic loaded stainless steel

Q. Li [a, b], F.K. Yan [a, c, *], N.R. Tao [a, **], D. Ponge [c], D. Raabe [c], K. Lu [a]

[a] Shenyang National Laboratory for Materials Science, Institute of Metal Research, Chinese Academy of Sciences, Wenhua Road 72, Shenyang, 110016, People's Republic of China
[b] School of Materials Science and Engineering, University of Science and Technology of China, Hefei, 230026, People's Republic of China
[c] Max-Planck-Institut fur Eisenforschung, Max-Planck Str. 1, D-40237, Düsseldorf, Germany

ARTICLE INFO

Article history:
Received 19 July 2018
Received in revised form
14 November 2018
Accepted 17 November 2018
Available online 20 November 2018

Keywords:
Nanotwins
Fatigue
Interface crack
Cyclic deformation
Austenitic steel

ABSTRACT

Cracks often initiate at phase boundaries in conventional second phase reinforced alloys during cyclic loading, which limits their fatigue properties. Here, we prepared a nanotwin strengthened 316L stainless steel consisting of nanotwinned and recrystallized grains by using plastic deformation and subsequent partial recrystallization annealing. Fatigue tests revealed that interfaces separating hard nanotwinned grains from soft recrystallized ones exhibited excellent resistance to crack initiation. More than half of the cracks (57% in number fraction) are found in recrystallized grains while a small fraction (11%) is observed at the interfaces between nanotwinned and recrystallized grains. This is ascribed to the elastic homogeneity and cyclic deformation compatibility between nanotwinned and recrystallized grains. At small cumulative cyclic strains (below 4000 cycles at $\sigma_a = 450$ MPa), nanotwinned grains deform compatibly with the recrystallized grains without noticeable strain localization at their interfaces. Nanotwins can accommodate cyclic plastic strains by interaction of dislocations with twin boundaries, especially through the motion of the well-ordered threading dislocations inside the twin lamellae. At large cumulative strains, a moderate strain gradient is developed in recrystallized grains surrounding nanotwinned grains as a function of distance from the interfaces due to the occurrence of localized deformation in nanotwinned grains. The nanotwinned grains show high microstructural stability without notable de-twinnning, thus retarding crack initiation and propagation. Therefore, improved fatigue property with high fatigue limit of ~350 MPa and high fatigue ratio of ~0.45 is achieved in the nanotwin strengthened stainless steel, which is better than that of conventional second phase reinforced steels with comparable strength.

1. Introduction

Introducing hard phases or inclusions into a soft matrix is an effective strategy to strengthen engineering alloys [1–6]. However, this kind of microstructure design often leads to failure initiation already at modest strains due to the preferential occurrence of interface cracking between hard phases and the soft matrix, especially in materials undergoing cyclic loading during service [5–8]. For example, in conventional martensite strengthened ferrite matrix dual phase (M-F DP) steels, cracks preferentially initiate at interphase boundaries at early loading stages (even at and below 10% of their lifetime) during fatigue tests [7], which significantly limits their fatigue life. This phenomenon originates in many multiphase alloys from the elastic inhomogeneity and plastic deformation incompatibility among the reinforcing stiff phases and the soft, elastically more compliant matrix [5,9–11]. Thus, those interfaces experience severe strain localization due to the presence of high densities of geometrically necessary dislocations required to accommodate the local mismatch in the plastic deformation, thereby promoting interface crack initiation [12,13].

* Corresponding author. Shenyang National Laboratory for Materials Science, Institute of Metal Research, Chinese Academy of Sciences, Wenhua Road 72, Shenyang, 110016, People's Republic of China.
** Corresponding author.
E-mail addresses: fkyan@imr.ac.cn (F.K. Yan), nrtao@imr.ac.cn (N.R. Tao).

https://doi.org/10.1016/j.actamat.2018.11.033
1359-6454/

Apparently, alleviating deformation incompatibility between hard and soft phases is one of the most effective methods to improve crack resistance of interphase boundaries during cyclic loading [5,7]. Previous investigations [5] indicated that by means of decreasing the carbon content of martensite in dual phase steels, the martensite can sustain a certain amount of strain at the expense of strength and thus deform in a more compatible fashion with the ferrite matrix, thereby enhancing the interface cracking resistance. Raabe et al. recently found that nano-sized austenitic reversion layers at the martensite/austenite interface in aged Fe−-Mn alloys can act as mechanical buffer regions impeding crack initiation and propagation [14–16]. However, for most heterogeneous phase reinforced materials, the capability of compatible deformation is very limited due to the different elastic modulus and the often intrinsic brittleness of the strengthening phases.

Different from conventional second phase strengthening, introducing high densities of deformation nanotwins into coarse grains by plastic deformation has proven efficient as a novel strategy to strengthen the soft matrix in some metals and alloys [17–19]. For example, Yan et al. [18] prepared a nanotwin strengthened 316L stainless steel (SS) which is mainly composed of a soft matrix of statically recrystallized (SRX) coarse grains containing dispersed hard nanotwinned grains by using dynamic plastic deformation (DPD) and subsequent partial recrystallization annealing. Different from conventional strengthening strategies that are based on using hard and stiff second phases, nanotwinned grains are very strong, ductile and leverage high work hardening capability [20]. Moreover, they are not only elastically matching to the adjacent SRX matrix without creating any phase boundary, but they also plastically co-deform in a compatible manner with the surrounding SRX grains up to a tensile strain of 5% [18]. This finding motivated a new microstructure design strategy of mixing recrystallized and nanotwinned grains, as the interfaces between them exhibit high fatigue cracking resistance. Also, nanotwinned grains provide good fatigue damage resistance due to their high strengthening capability and microstructural stability associated with the underlying dislocation-twin boundary interactions during cyclic loading [21–26]. Hence, this kind of single-phase duplex microstructure, i.e. hard nanotwinned grains embedded in a matrix of soft SRX grains, is more attractive than conventional second phase reinforced materials for improving fatigue properties. Here, we implement and study this microstructure design strategy in a nanotwin strengthened 316L SS with the aim to better understand its response to cyclic deformation and the associated damage mechanisms when exposed to fatigue tests. Especially, the characteristics of nanotwinned/SRX grain interfaces and the stability of nanotwins will be further investigated.

2. Experimental

The material is a commercial AISI 316L austenitic stainless steel (SS) with composition Fe-16.11Cr-10.00Ni-2.01Mo-1.43Mn-0.38Si-0.039P-0.012S-0.011C (*wt.%*). The hot-forged 316L SS was solution heat-treated at 1473K for 1 h and then water quenched to obtain a uniform austenitic structure with 65 μm average grain size. Then the coarse grained (CG) 316L SS samples were processed on a dynamic plastic deformation (DPD) facility at a strain rate of 10^2–10^3 s^{-1} at room temperature [19]. Cylindrical CG samples with a diameter of 24 mm and height of 10 mm were impacted to a cumulative strain of $\varepsilon = 0.8$ (DPD 316L SS samples). The deformation strain is defined as $\varepsilon = \ln(L_o/L_f)$, where L_o and L_f are the initial and final thickness, respectively. The final thickness of DPD treated samples was ~4.5 mm and the diameter was ~36 mm, which was large enough to perform stress-controlled push-pull fatigue tests. These DPD 316L SS samples were subsequently annealed at 770 °C for 90 min and then water quenched, to obtain nanotwin strengthened 316L SS. Mechanical properties and microstructural evolution of the DPD and annealed-DPD 316L SS (nanotwin strengthened 316L SS) were systematically studied as presented in Refs. [19,21,27].

Symmetrical stress-controlled push-pull fatigue tests (stress ratio $R = -1$) were performed on an Instron E3000 machine with a sinusoidal wave at a frequency of 20 Hz. Fatigue specimens were cut from the nanotwin strengthened 316L SS into a plate-type dog-bone shape with a gauge section of 2.2×2 mm^2 and a length of 5 mm using an electrical spark machine. Prior to fatigue testing, the specimens were ground using SiC grit papers from $400^{\#}$ to $5000^{\#}$ and then electro-polished in order to observe the microstructures also after the fatigue tests. Ex-situ fatigue tests were also performed for 1000, 4000, 7000, 13000 interrupted cycles at a high stress amplitude of 450 MPa for microstructure analysis.

The cyclic deformation and damage microstructures of the fatigue deformed specimens were characterized by a scanning electron microscope (SEM) FEI Verios 460 with electron channeling contrast (ECC) imaging, a Zeiss-Crossbeam XB 1540 FIB-SEM with electron backscatter diffraction (EBSD) mapping and a transmission electron microscope (TEM) JEOL 2010 operated at 200 kV. All the SEM and TEM observations take a perspective of longitudinal cross-sections at locations away from the facture surface. TEM foils were sliced from the longitudinal cross-section of the gauge section and mechanically thinned to 30 μm, and then twin-jet electro-polished in an electrolyte of 8% perchloric acid and 92% alcohol at −15 °C. The deformation gradient in SRX grains surrounding nanotwinned grains after fatigue fracture was analyzed using the kernel average misorientation (KAM) measure which maps an approximate measure for the geometrically necessary dislocation density to roughly display local strain gradients in each grain [28,29]. Grain reference orientation deviation (GROD) maps were also used to display long-range strain gradients within every grain based on the calculation of angular deviations from the reference pixel having the lowest KAM within a given grain [29,30].

3. Results

3.1. Microstructures of nanotwin strengthened 316L SS

DPD processing induced a mixed nanostructure consisting of nanograins, nanotwins and dislocation substructures in the 316L SS, as described in Ref. [21]. Subsequent annealing at 770 °C for 90 min led to a partial static primary recrystallization of the deformation structure, forming a single austenitic phase nanotwin strengthened 316L SS. As shown in Fig. 1, the microstructure is mainly composed of SRX coarse grains and two types of non-recrystallized regions, namely retained nanotwinned (NT) grains and blocks of dislocation structures (DS). The SRX grains exhibit a random orientation distribution (Fig. 1b). They are nearly equiaxed with an average grain size of ~5.5 μm, constituting ~67% in volume. Most nanotwinned grains exhibit a larger grain size compared with SRX grains, ranging from a few to several tens of micrometers. They contain a high density of twin lamellae with an average thickness of $\sim 36 \pm 3$ nm as quantified by TEM. Nanotwinned grains occupy a total volume fraction of ~ (26 ± 5) % as revealed by SEM characterization. According to the EBSD analysis (Fig. 1b), the nanotwins show a rough <111>//DPD compression direction relationship. This is consistent with our previous investigation [27] that most twin planes are roughly parallel to the loading direction with the orientation of approx. ~19° between them in the annealed DPD sample. The dislocation structures (constituting ~7% in volume) are typical recovered dislocation tangles, walls and cells, which are common in deformed 316L SS [21]. TEM images (Fig. 1c) show that

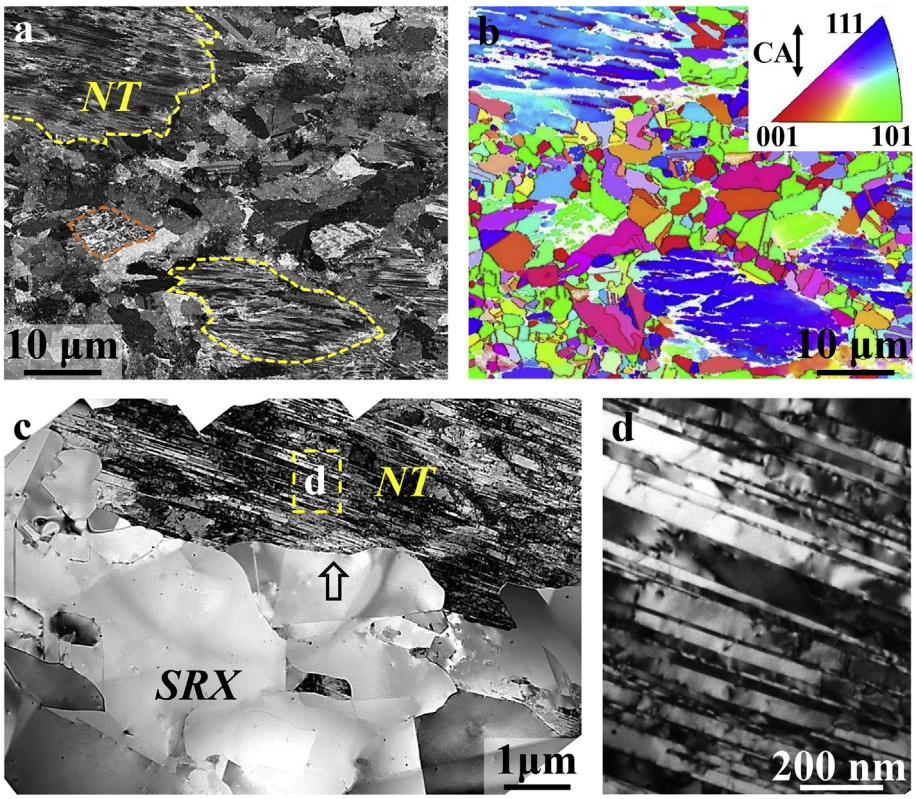

Fig. 1. (a) A typical cross-sectional SEM-ECC image showing nanotwinned grains (NT, outlined by yellow dotted line) and dislocation substructures (outlined by orange dotted line) embedded in statically recrystallized (SRX) grains in a nanotwin strengthened 316L sample. (b) The corresponding EBSD inverse pole figure of (a) along the compression axis (CA, i.e. DPD direction). Bright-field TEM images showing (c) SRX grains embedded with nanotwinned grains and (d) twin/matrix lamellae with a low density of dislocations. (For interpretation of the references to color in this figure legend, the reader is referred to the Web version of this article.)

the SRX grains are nearly devoid of dislocations. Specifically, the interfaces between SRX grains and nanotwinned grains are clear and sharp without any noticeable dislocation populations (as arrowed in Fig. 1c). There are still many dislocations inside the nanotwinned grains (Fig. 1d), but their overall dislocation density is much lower (an order of magnitude [31]) in comparison with that in the DPD treated samples. This single phase nanotwin strengthened 316L SS exhibits an excellent combination of strength and ductility with the yield strength of ~526 MPa and the uniform elongation of ~29%.

3.2. Fatigue damage morphology and cracking behavior

The surface deformation morphologies of the nanotwin strengthened 316L SS after fatigue fracture at both low and high stress amplitudes are shown in Fig. 2. At a low stress amplitude of $\sigma_a = 350$ MPa (Fig. 2a–b) we found characteristic intrusions and extrusion (I/Es) which are derived from slip bands [32,33] in several SRX grains adjacent to nanotwinned grains. Here, those neighboring SRX grains are defined as one or two layers of SRX grains surrounding centered nanotwinned grains, within approx. 0–11 μm away from the nanotwinned/SRX grain interfaces. In contrast, no obvious I/Es were observed in SRX grains far away from nanotwinned grains. Those remote SRX grains are defined as approx. 11 μm or more away from interfaces, i.e., beyond two layers of SRX grains surrounding nanotwinned grains. Most nanotwinned grains were intact with sporadic zig-zag slip bands intersecting with twin lamellae. Such inhomogeneous distribution of deformation damage features is more significant at $\sigma_a = 450$ MPa. As shown in Fig. 2c–d, more and severe I/Es occurred in SRX grains close to nanotwinned grains. However, SRX grains remote from the nanotwinned grains exhibited weak damage with only a few I/Es. In nanotwinned grains, stripped shear bands also accompanied by I/Es (referred to as persistent slip band-like shear bands [21]) were observed. These shear bands were aligned along or intersected twin boundaries, extending over a length of several to dozens of micrometers. Some I/Es induced by shear bands were interrupted by twin boundaries and confined in a local region of nanotwinned grains. These observations indicated that the cyclic deformation damage in SRX grains located close to nanotwinned grains was more severe than those placed far away from nanotwinned grains on the verge of failure, a feature which influenced the fatigue cracking behavior.

As shown in Fig. 3a–d, fatigue cracks initiated in SRX grains, nanotwinned grains and nanotwinned/SRX interfaces in fatigued samples at $\sigma_a = 450$ MPa, yet their distribution was inhomogeneous. In order to compare the fatigue crack resistance of SRX grains, nanotwinned grains and nanotwinned/SRX interfaces, we counted the number of well-developed cracks according to their initiation sites by SEM-ECC observations. For example, if a crack initiated and propagated only in SRX grains, then it can be definitely counted as one single and percolative well-developed crack which initiated in SRX grains (as shown in Fig. 3a). According to 147 cracks counted in several fatigued samples (Fig. 3d), more than half of the cracks (~57% in number fraction) occurred in SRX grains. These cracks often initiated and propagated along I/Es, such as often observed in coarse grained materials [33]. It is noteworthy that the number fraction of cracks (~45%) in those SRX grains adjacent to nanotwinned grains (Fig. 3a) is much higher than that in SRX grains placed more remote from nanotwinned grains (~12%).

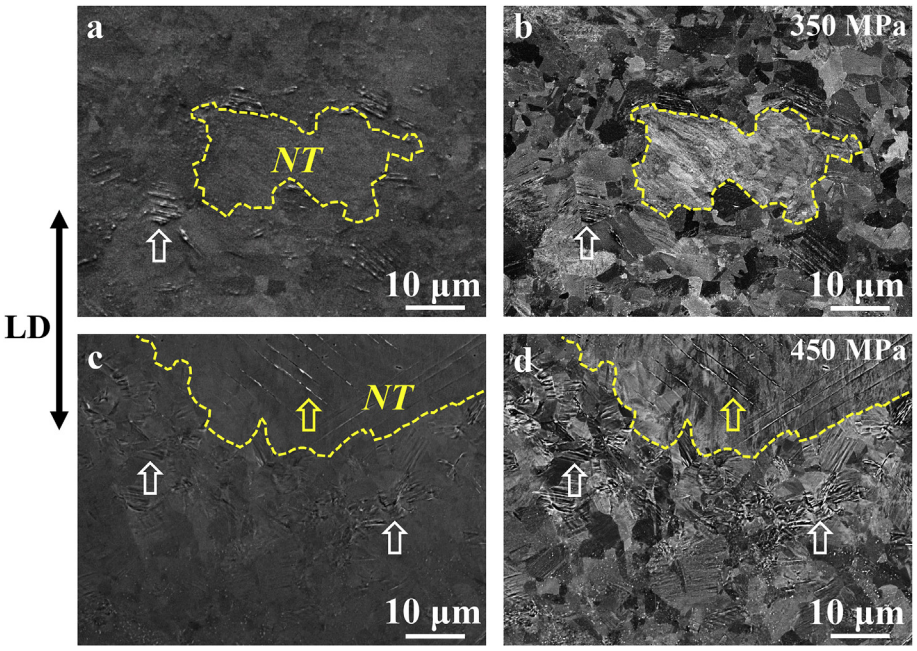

Fig. 2. Typical SEM-SE (a, c) and corresponding SEM-ECC (b, d) images of longitudinal cross-section at the locations away from the fracture surface showing fatigue damage morphologies of nanotwin strengthened 316L sample after fatigue fracture at (a, b) $\sigma_a = 350$ MPa ($N_f = 10341124$ cycles) and (c, d) $\sigma_a = 450$ MPa ($N_f = 26192$ cycles), respectively. Intrusions and extrusions (I/Es) in SRX grains are arrowed in white and shear bands in nanotwinned grains are arrowed in yellow. (For interpretation of the references to color in this figure legend, the reader is referred to the Web version of this article.)

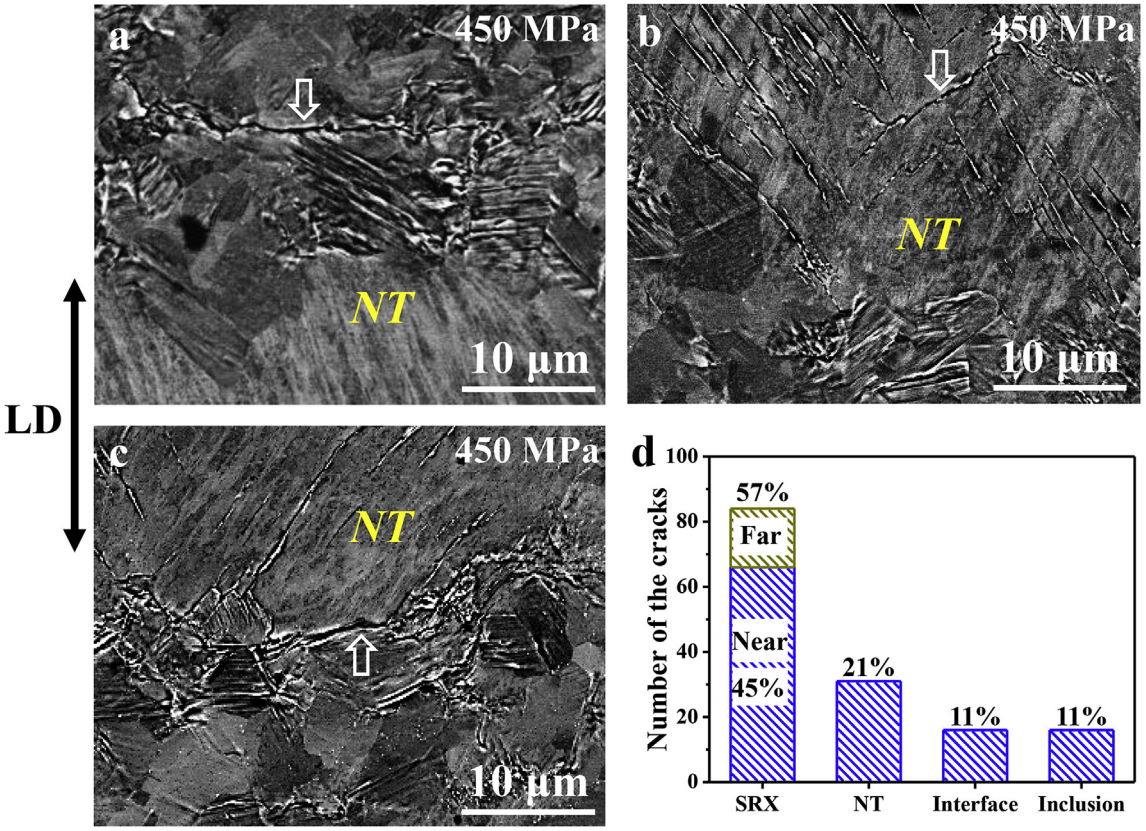

Fig. 3. Typical SEM-ECC cross-sectional observations showing typical fatigue cracks (arrowed) initiation and propagation in (a) SRX grains close to interfaces, (b) nanotwinned grains and (c) at the nanotwinned/SRX grain interfaces after fatigue fracture at $\sigma_a = 450$ MPa ($N_f = 26192$ cycles). (d) Statistic distribution of fatigue cracks among these microstructures.

This is consistent with the above finding that more I/Es occurred in neighboring SRX grains than that in remote ones. A fraction of ~21% cracks are observed in nanotwinned grains. Those fatigue cracks initiated and propagated along I/Es in nanotwins, along or intersecting with twin boundaries. Crack propagation in nanotwinned grains was associated with multiple kinks and branches due to the interruption of cracks by twin boundaries. Moreover, the crack propagation orientation is macroscopically vertical to the loading direction in the SRX grains (arrowed in Fig. 3a) but inclined to the loading direction in the nanotwinned grains (arrowed in Fig. 3b), implying a lower propagation rate for cracks in nanotwinned grains [34].

Interestingly, most of the nanotwinned/SRX grain interfaces remain intact (Fig. 2b, d) and do not exhibit significant macrocracks (Fig. 3c). Only a small fraction (~11%) of fatigue cracks were found at interfaces (Fig. 3d). Most of interface cracks were at the initiation stage with several micrometers along the interfaces (Fig. 3c). It seemed that the impingement among interfaces and I/Es in SRX grains or shear bands in nanotwinned grains promoted crack initiation.

3.3. Cyclic deformation microstructure of SRX grains revealed by TEM characterization

To characterize the fatigue deformation microstructure of nanotwin strengthened 316L SS after fracture at both low and high stress amplitudes, SRX grains surrounding nanotwinned grains were examined by TEM, as shown in Fig. 4 and Fig. 5. For imaging and comparing the dislocation configurations in different SRX grains, many SRX grains were tilted into the <110> zone axis. At $\sigma_a = 350$ MPa, the dislocation density in SRX grains close to nanotwinned grains is slightly higher than that in remote ones. Moreover, typical dislocation walls occurred in several of the neighboring SRX grains (Fig. 4b) [35,36]. In the more remote SRX grains, primary planar dislocations were observed (Fig. 4c and d) [36].

At a stress level of $\sigma_a = 450$ MPa, the dislocation density accordingly increased and the difference in the evolved dislocation configurations was more significant between the nanotwin-neighboring and the remote SRX grains. As shown in Fig. 5a–d, well-developed dislocation cells and walls (marked with open arrows in Fig. 5a) are formed in many SRX grains adjacent to nanotwinned grains. Specifically, some first-neighboring SRX grains (outlined in Fig. 5a) were refined into subgrains (marked with solid arrows in Fig. 5a) with an average size of ~700 nm (Fig. 5b), which evolved from dislocation cells and walls [35]. Also, in neighboring SRX grains, some newly-formed stacking faults (marked with open triangles in Fig. 5c) were observed. In contrast, within SRX grains away from nanotwinned grains, dislocations were arranged in forms of dense tangles, dislocation networks and the early-developing dislocation walls (Fig. 5d). Also, no stacking faults were observed in them. Such inhomogeneous distribution of dislocation configurations indicated that the fatigue deformation was more severe in SRX grains which were close to nanotwinned grains than in those more remote after fracture, consistent with the SEM observations. Obviously, a strain gradient exists in a large region of the SRX grains as a function of distance from the nanotwinned/SRX grain interfaces.

3.4. Strain gradient development

In order to investigate the strain gradient development in SRX grains surrounding nanotwinned grains, ex-situ interrupted fatigue tests with a stress amplitude of $\sigma_a = 450$ MPa were performed

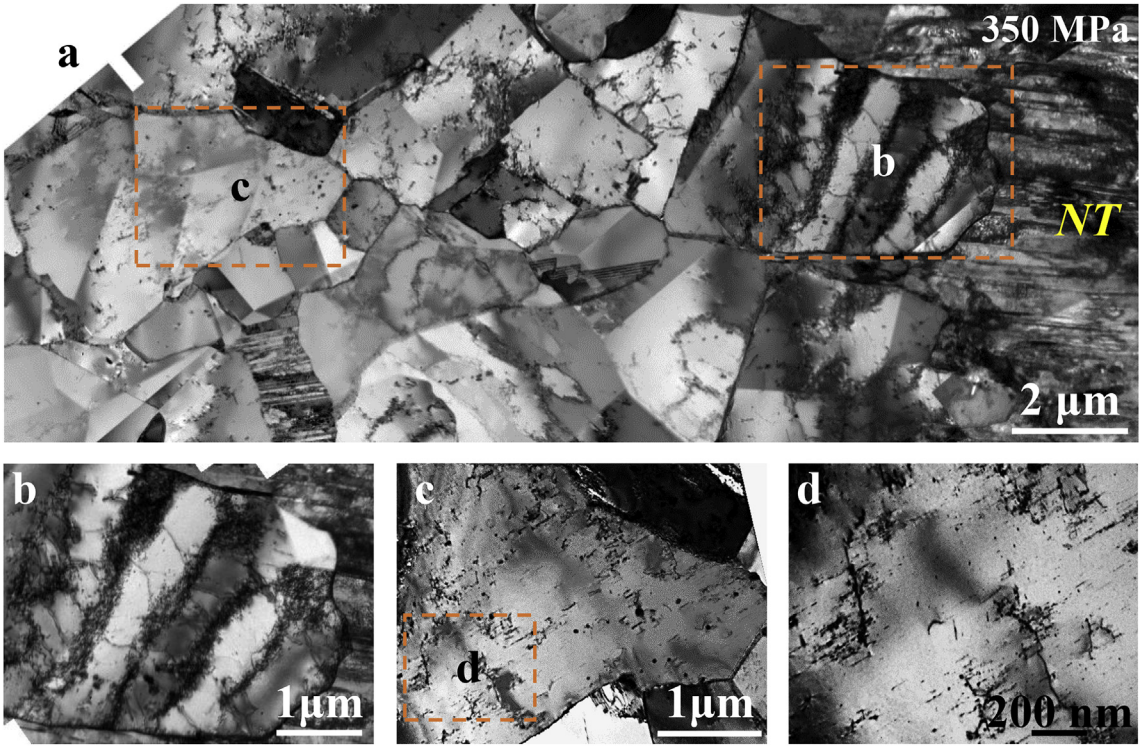

Fig. 4. Typical bright-field TEM images showing the deformation microstructure after fatigue fracture at $\sigma_a = 350$ MPa ($N_f = 10341124$ cycles). (a) SRX grains are divided into two regions: close to (one or two layers of SRX grains) and far away from (beyond two layers of SRX grains) the nanotwinned/SRX grain interfaces. (b) Typical dislocation walls in neighboring SRX grains and (c) typical planar dislocation arrays in more remote SRX grains. (d) Close observation of the rectangle in (c). All SRX grains in (b–d) are tilted to the <110> zone axis.

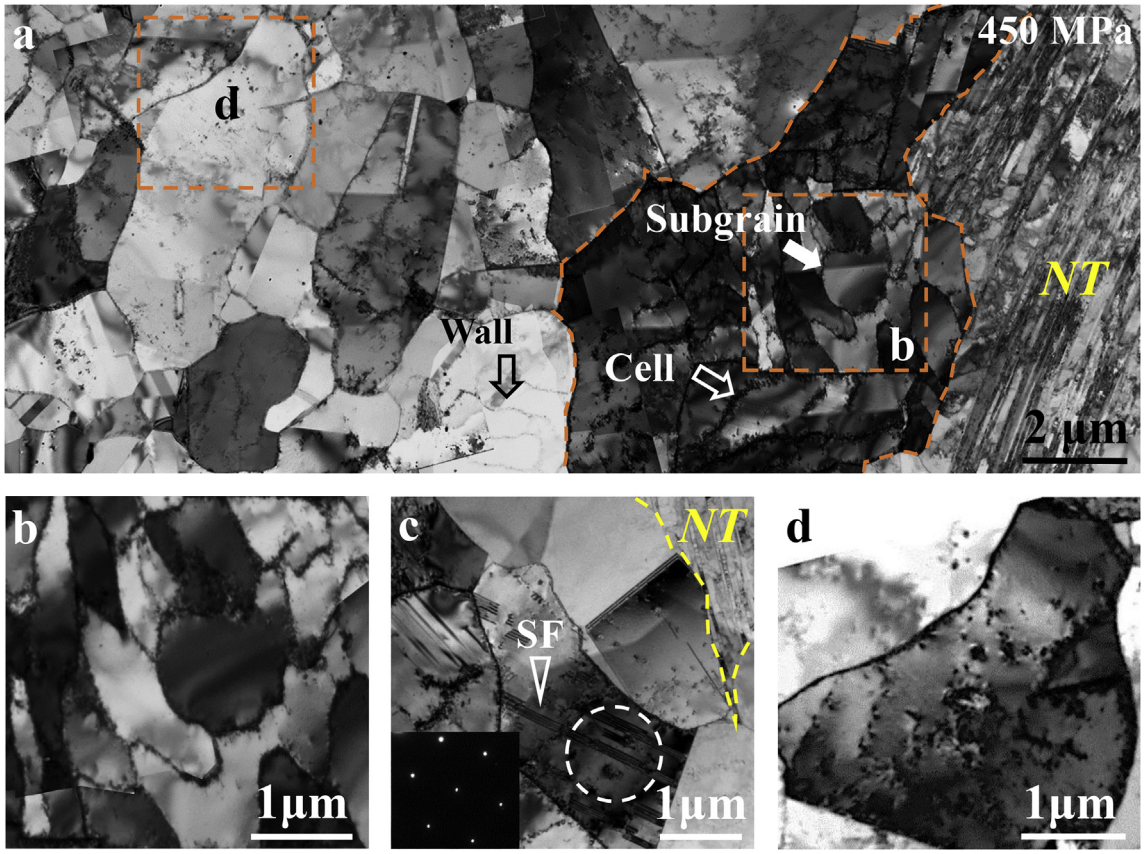

Fig. 5. (a) A typical bright-field TEM image showing the deformation microstructure after fatigue fracture at $\sigma_a = 450$ MPa ($N_f = 8743$ cycles). Well-developed subgrains in the first neighboring SRX grain are marked with solid arrows, and dislocation cells and walls are marked with open arrows. (b) Close observation of subgrains and (c) stacking faults in neighboring SRX grains (marked with open triangles) and (d) dislocation tangles and walls in remote SRX grains. All SRX grains in (b–d) are tilted to the <110>zone axis.

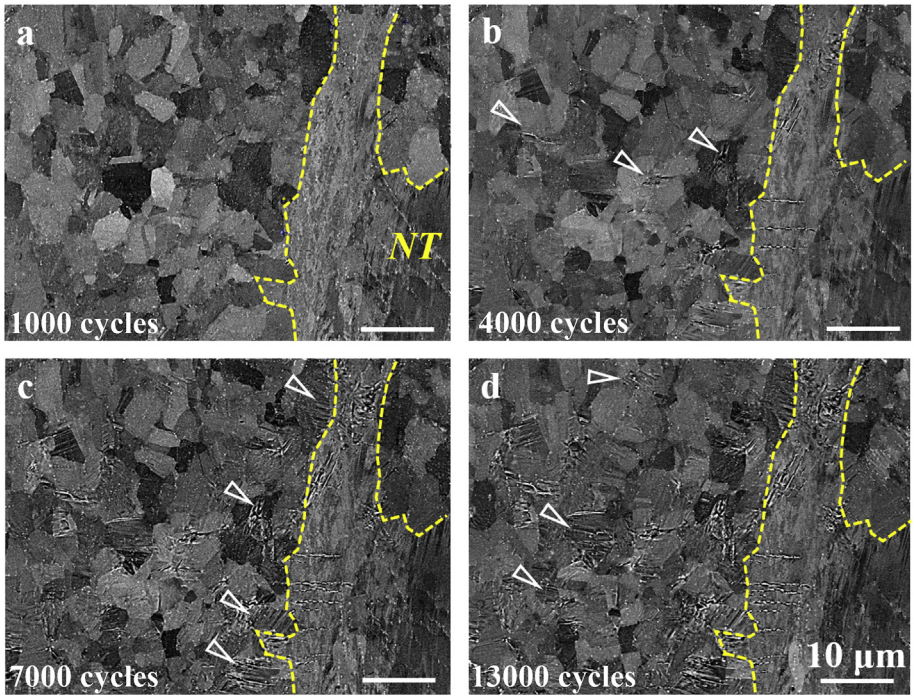

Fig. 6. SEM-ECC images showing the fatigue damage surface morphologies of SRX grains surrounding the nanotwinned grain during ex-situ fatigue tests at $\sigma_a = 450$ MPa for different cycles: (a) 1000 cycles, (b) 4000 cycles, (c) 7000 cycles, (d) 13000 cycles. The specimen failed at 14120 cycles. Intrusions and extrusioins (I/Es) in SRX grains are marked with triangles.

(Fig. 6a–d). At the early stage of 1000 cycles (Fig. 6a), SRX grains, no matter close to or away from nanotwinned grains, exhibited uniform deformation. No notable damage feature was observed both in SRX grains and nanotwinned grains. With increasing the load scenario to 4000 cycles (Fig. 6b), sporadic I/Es (indicated by triangles) occurred in both nanotwin-neighboring and remote SRX grains. No obvious deformation features concentrated at the nanotwinned/SRX grain interfaces. TEM observations (Fig. 7a–c) showed that most SRX grains exhibited a roughly comparable dislocation density. Typical planar dislocation arrays were observed both in nanotwin-neighboring SRX grains (Fig. 7b) and remote ones (Fig. 7c), much like in conventional materials [35,36]. No additional dislocation populations concentrating at the nanotwinned/SRX grain interfaces (arrowed in Fig. 7b) were observed compared with SRX/SRX grain boundary regions (arrowed in Fig. 7c). At small cyclic strains, nanotwins co-deformed compatibly with the surrounding SRX grains without generating notable strain gradients inside the adjacent SRX grains.

With further increasing the accumulative deformation to 7000 cycles (Fig. 6c), more and more I/Es (marked with triangles in Fig. 6c) occurred in the neighboring SRX grains than in the more remote SRX grains, indicating that a strain gradient was developed over the SRX grain region surrounding nanotwinned grains as a function of distance from the interfaces. The density of the shear band-induced I/Es also increased in the nanotwinned grains. After 13000 cycles (Fig. 6d, the sample failed at 14120 cycles), some new I/Es (indicated by triangles) formed in SRX grains remote from nanotwinned grains, yet the I/Es density slightly changes in neighboring SRX grains and nanotwinned grains. This observation suggests that the deformation gradient extended also into the more remote regions. Such inhomogeneous deformation of SRX grains is also covered by SEM and TEM observations (Figs. 2–5 and Fig. 6c–d) after fatigue to fracture. Hence, a strain gradient is gradually developed within the SRX grain region as a function of distance from the nanotwinned/SRX grain interface with cumulative cyclic strains, then extend into larger environmental-regions around the nanotwinned grains.

The macroscopic strain localization and strain gradient distribution in these microstructures were evaluated in terms of KAM and GROD maps of the nanotwin strengthened 316L SS sample after fatigue to fracture at $\sigma_a = 350$ MPa. Fig. 8b shows the heterogeneously distributed KAM value between SRX grains and nanotwinned grains. The KAM value in nanotwinned grains is higher than that observed in SRX grains due to the occurrence of shear band-induced strain localization within nanotwinned grains [28]. For SRX grains, the KAM values in all near-grain boundary regions are slightly higher than in their grain interiors, as observed in conventional coarse grained alloys [9,37]. Specifically, the KAM values in the interior of the SRX grains close to the nanotwinned/SRX grain interfaces (indicated by arrows) are nearly identical to that in near-SRX grain boundary regions. This means that the strain localization in SRX grains around nanotwinned/SRX grain interfaces was mild. The GROD map in Fig. 8c further reveals the long-range strain and orientation gradients among the SRX grains along the nanotwinned/SRX grain interfaces. Some SRX grains adjacent to nanotwinned/SRX grain interfaces (arrowed) show slightly higher orientation deviations (color in green) than those far away from the interfaces (color in blue), implying the development of strain gradients in SRX grains surrounding nanotwinned grains. The GROD value of most SRX grains is around 0–1° translating to a moderate strain gradient, much lower than in a quenched martensite-ferrite dual phase steel in which the GROD value is already as high as ~5–8° before plastic deformation [30].

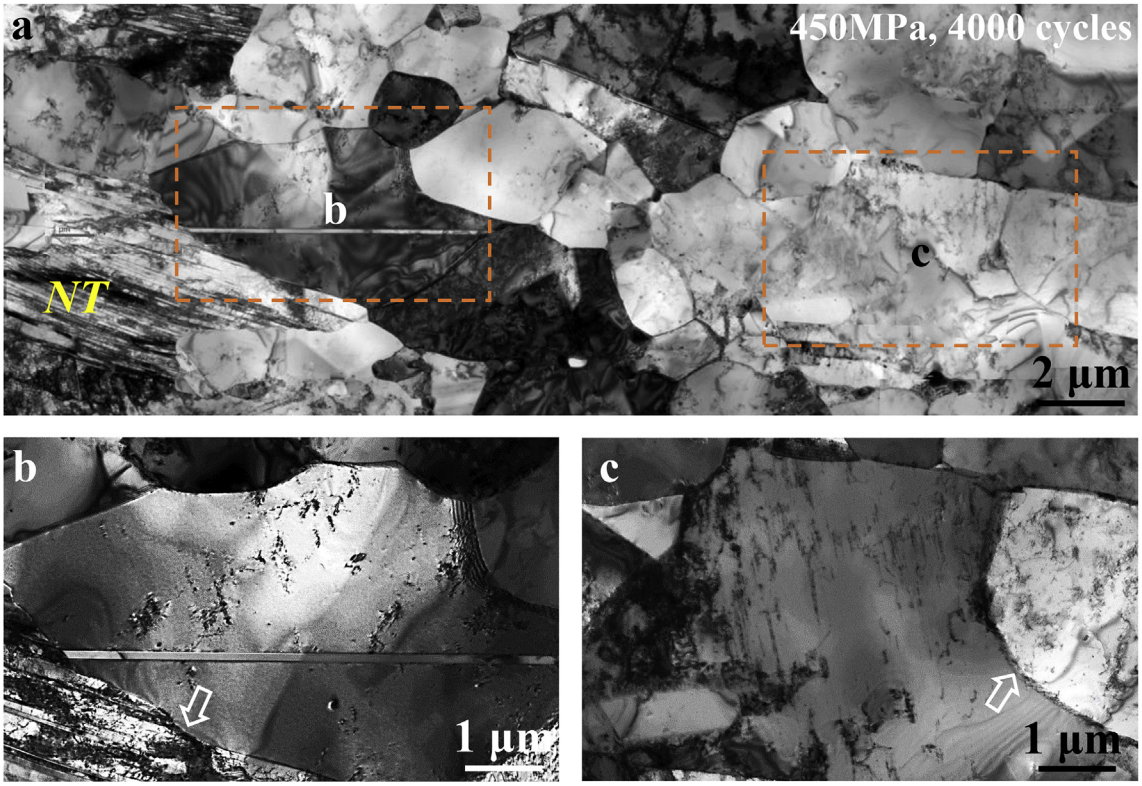

Fig. 7. (a) A typical bright-field TEM image showing the deformation microstructure of SRX grains surrounding the nanotwinned grain after 4000 cycles at $\sigma_a = 450$ MPa. Typical planar dislocation arrays occurred in both (b) neighboring and (c) more remote SRX grains. SRX grains in (b) and (c) are tilted to the <110> zone axis.

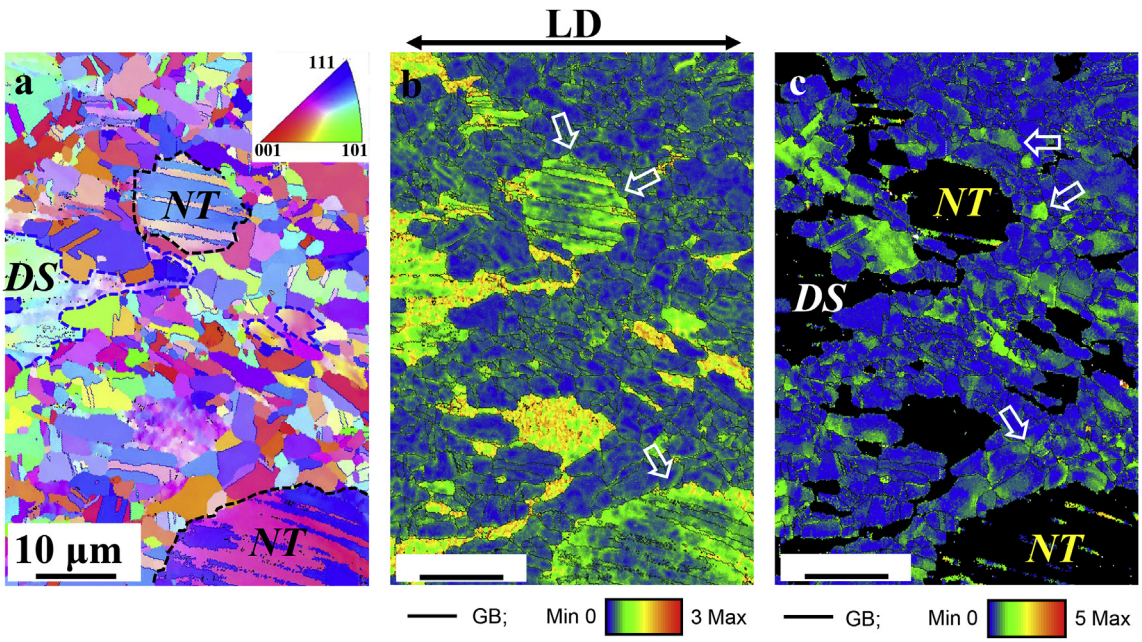

Fig. 8. (a) A typical EBSD inverse pole figure showing the microstructure of nanotwin strengthened 316L samples after fatigue fracture at $\sigma_a = 350$ MPa ($N_f = 10341124$ cycles). (b) The corresponding kernel average misorientation (KAM) map showing the heterogeneous distribution of KAM values between SRX and nanotwinned grains. (c) The corresponding grain reference orientation deviation (GROD) map showing the moderate strain gradient development in SRX grains. The arrows in (b) and (c) show the typical features around nanotwinned/SRX grain interfaces.

3.5. Deformation of nanotwinned grains by TEM characterization

At small cyclic strains (below 4000 cycles at $\sigma_a = 450$ MPa), nanotwinned grains can sustain the cyclic strains through dislocation-twin boundary interactions (Fig. 9a). Specifically, we observed a series of threading dislocation segments along twin boundaries under a two-beam diffraction vector of $\mathbf{g} = [200]$ (Fig. 9b). These threading dislocations regularly arrayed and laid parallel to each other, belonging to a single-slip system. The well-ordered threading dislocations are analogous to the correlated necklace dislocations observed in growth nanotwinned Cu under cyclic loading [22], which may significantly contribute to the cyclic strains.

At large cyclic strains, localized deformation of nanotwinned grains occurred in the form of shear banding against twin lamellae. For instance, after fatigued to failure at $\sigma_a = 350$ MPa, deformation localization initiated in narrow shear bands (roughly ~100–500 nm) within which high density of dislocations were presented (Fig. 9c). With increasing the stress amplitude to 450 MPa (to failure), the cumulative cyclic strains were larger and thus led to thickening of shear bands (over ~500 nm). Dislocation substructures and nano-sized elongated grains formed within the well-developed shear bands (Fig. 9d). The evolution of shear band-induced localized deformation of nanotwins was reported in Cu-Al alloys [38]. Also, a few thick twin lamellae were locally fragmented. However, most nanotwins were still intact and stable without significant coarsening of the twin lamellae (still averagely 36 ± 2 nm) after fatigue to fracture.

4. Discussion

According to the microstructure characterization, most cracks initiate in SRX grains rather than at interfaces between nanotwinned and SRX grains. The nanotwinned/SRX grain interfaces are more resistant to crack initiation. This is different from hard phase reinforced alloys in which hetero-phase boundaries are preferential sites for crack initiation [5–8]. High cracking resistance of the nanotwinned/SRX grain interface is ascribed to the elastic homogeneity and cyclic deformation compatibility between nanotwinned grains and the surrounding SRX grains. The nanotwinned grains can co-deform compatibly with the surrounding SRX grains at small cumulative strains (below 4000 cycles at $\sigma_a = 450$ MPa). Strain localization can be reduced by forming moderate strain gradients in the SRX grains at high accumulative cyclic strains (Fig. 8). The intrinsic cyclic deformation mechanisms associated with the interactions between the dislocations and the nanotwins and the strain gradient development in the surrounding SRX grains are key factors to understand the fatigue behavior of the nanotwin strengthened 316L SS.

4.1. Cyclic deformation mechanism of nanotwinned grains

Nanotwinned grains exhibited very limited ductility due to the presence of a high density of dislocations within them after DPD processing [21,31,39]. Subsequent annealing led to significant reduction of the dislocation density (up to an order of magnitude [31]) through dislocation rearrangements and annihilation inside nanotwinned grains. Nanotwinned grains then provided ample room for dislocation slip and accumulation to regain the deformation capability (Fig. 9a). Since the twin boundaries were roughly parallel to the loading direction (Fig. 1b), a series of single-slip well-ordered threading dislocations were activated in some twin lamellae. They may slip collectively back and forth within confined twin lamellae during cyclic loading, like correlated necklace dislocations observed in growth nanotwinned Cu [22]. Those well-ordered dislocations can carry large fractions of the imposed cyclic strains and preserve the stability of the nanotwins [22,23].

With increasing the cumulative cyclic strains, the stored dislocation density in nanotwins was so high that nanotwins were exhausted to accommodate further cyclic strains by dislocation slip [18]. Specifically, reversal slip of the well-ordered threading dislocations within the twin lamellae was interrupted and/or impeded

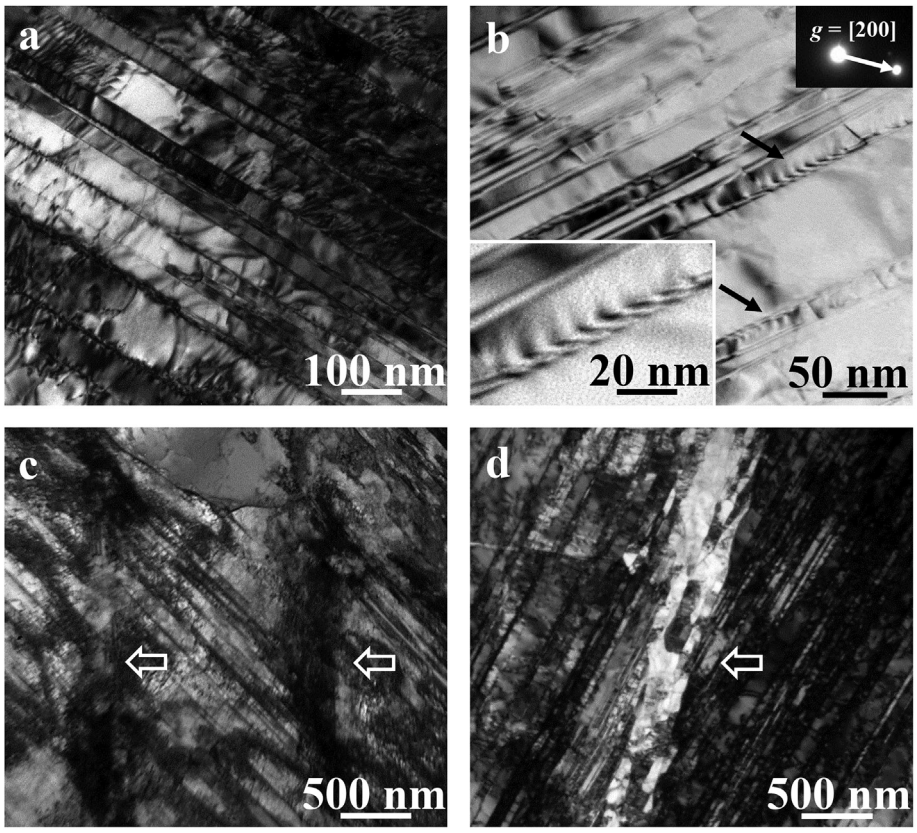

Fig. 9. Bright-field TEM images showing the deformation evolution of nanotwinned grains during cyclic loading. Nanotwinnd grains can deform at small accumulative strains (4000 cycles at $\sigma_a = 450$ MPa) by (a) the typical dislocation-twin boundary interactions and (b) the well-ordered threading dislocations (arrowed, enlarged in the bottom-left inset) observed under a two-beam diffraction vector of $\mathbf{g} = [200]$ (the top-right inset). Strain localization in terms of shear bands occurred in nanotwins at large accumulative strains: (c) nucleation of shear bands (arrowed) in samples fatigued to failure at $\sigma_a = 350$ MPa and (d) thickening of shear bands (arrowed) in samples fatigued to failure at $\sigma_a = 450$ MPa.

by the accumulating dislocations. The extra cyclic strains were then introduced into shear bands intersecting with twin lamellae. These shear bands governed the deformation localization response of the nanotwinned grains. The shear bands were thickening accompanied by the formation of dislocation substructures and nanosized grains within them with accumulating strains (Fig. 9c–d). This phenomenon was different from growth nanotwinned Cu in which severe de-twinning governed deformation localization at high cyclic strains [23,40–43]. Most nanotwins in nanotwinned Cu were coarsening and many of them were even dissolved upon cyclic loading [40–43]. In contrast, in the current steel most deformation nanotwins were very stable without pronounced twin lamellae coarsening or de-twinning, although many shear bands formed inside the nanotwinned grains. This is attributed to the fact that numerous pre-existing sessile dislocations at twin boundaries inhibited the movement of Shockley partial dislocations along them [21,43]. Furthermore, the cyclic mechanism of nanotwins is also influenced by the twin thickness [44–46] and stacking fault energy [47]. The twin boundary spacing in nanotwin strengthened 316L SS (~36 nm) was much larger than in nanotwinned Cu (~4–11 nm) [41], which also suppressed de-twinning [41,44–46].

4.2. Compatible cyclic deformation and strain gradient development in SRX grains

As nanotwinned grains possess the same elastic modulus and co-deform compatibly together with the surrounding SRX grains, no pronounced geometrically necessary dislocations will generate at nanotwinned/SRX grain interfaces at small cyclic strains (Fig. 7b). The interfaces were mechanically similar to conventional iso-phase grain boundaries without specific additional strain localization due to the low mechanical contrast across them. This applies even over a load range of 4000 cycles at 450 MPa (Fig. 6a and b). This is different from second phase reinforced alloys which exhibit inhomogeneous deformation between the reinforcements and the soft matrix throughout the whole cyclic deformation [9–11]. For example, in ferrite-martensite dual phase steels, localized strains were introduced at ferrite/martensite interfaces already during the first loading cycle [11]. The discrepancy of the elastic modulus and the sharp ductility-mismatch between the ferrite and the martensite resulted in the intense strain localization at interfaces and the high strain gradient in ferrites [5,9–11,30].

With increasing the cyclic strain, shear bands occurred in nanotwinned grains (Fig. 9c and d). Such localized deformation (see 4.1) in the nanotwinned regions unavoidably induced strain localization at nanotwinned/SRX grain interfaces, which in turn generated strain gradients within the SRX grains surrounding the nanotwinned grains. TEM and SEM characterization revealed the strain gradient-induced inhomogeneous deformation of the SRX grains as a function of distance from interfaces (Figss. 4–6). Dislocation cells, walls, even subgrains formed in the neighboring SRX grains while the more remote SRX grains displayed typical dislocation arrays due to the activation of essentially one single slip system [36] (Figs. 4 and 5). It is noteworthy that the strain localization and strain gradient built up around nanotwinned grains are less pronounced (Fig. 8) than in alloys reinforced by second phases [11,28,30]. The compatible cyclic deformation between nanotwinned and SRX grains at small cyclic strains postponed the strain

localization around interfaces. The rapid work hardening of SRX grains (due to the low stacking fault energy for 316L SS) effectively transferred the strain gradients into more remote SRX grains, thereby remedying the deformation incompatibility. This unique cyclic deformation mechanism markedly retarded the crack initiation and propagation.

4.3. High fatigue crack resistance of nanotwinned/SRX grain interfaces

Fatigue cracks often initiate at phase boundaries in second-phase reinforced alloys [5–8]. However, in the nanotwin strengthened 316L SS, over half of the cracks occurred inside the SRX grains (57% in number fraction) rather than at the nanotwinned/SRX grain interfaces (11%) (Fig. 3d), implying higher fatigue cracking resistance of the latter. The low strain localization around interfaces and the moderate strain gradient within surrounding SRX grains inhibit fatigue cracking at interfaces. On the contrary, the neighboring SRX grains severely deformed with intense I/Es in the late stage of fatigue, which resulted in significant cracking within them.

Also, most twin lamellae were stable without obvious thickening. No severe de-twinning occurred in nanotwins near nanotwinned/SRX grain interfaces, which suppressed the generation of cracking at interfaces. This is different from growth nanotwinned Cu in which intensive de-twinning and coarsening occurred around the adjacent columnar grain boundaries [23,40–43]. Such strain localization-induced softening resulted in cracking along columnar grain boundaries [40–43]. The high fatigue crack resistance of the nanotwinned/SRX grain interfaces improved the fatigue properties of nanotwin strengthened 316L SS.

4.4. Good fatigue properties

The results and analyses above indicated that deformation compatibility of nanotwin strengthened 316L SS was much improved in comparison with second phase reinforced alloys. The nanotwinned/SRX grain interfaces exhibited an enhanced fatigue cracking resistance due to the alleviation of strain localization around them. Hence, an improved fatigue property is achieved in nanotwin strengthened 316L SS. The Wöhler S-N curves (Fig. 10a) and Table 1 reveal that the fatigue strength increases significantly. The fatigue limit (σ_f, i.e. the fatigue strength at a cycling lifetime $\geq 10^7$ cycles) reaches up to 350 MPa, ~75% higher than coarse grained 316L SS (~200 MPa). Such fatigue property was also superior to the traditional ferrite-martensite DP steels (DP 600 and 590). The fatigue limit is expected to increase proportionally to tensile strength (σ_{UTS}) during the stress-controlled fatigue [48–51], which is defined as fatigue ratio (σ_f/σ_{UTS}). As shown in Table 1, the fatigue ratio of nanotwin strengthened 316L SS is as high as ~0.45, higher than that of coarse grained, nanostructured equal channel angular pressing (ECAP) and DPD treated 316L SS and ferrite-martensite DP steels in which it ranges from 0.33 to 0.40 [21,49,53,54,56]. This means that the fatigue limit of nanotwin strengthened 316L SS is higher than that of DP steels with comparable tensile strength.

The stress-controlled fatigue behavior can be described by an empirical Basquin equation as [52]:

$$\sigma_a = \sigma_f'(2N_f)^b \quad (1)$$

Where N_f is the number of cycles to failure, σ_f' is the fatigue strength coefficient (related to tensile strength) and b is the fatigue strength exponent, respectively. According to this equation, the fatigue strength exponent (b) of nanotwin strengthened 316L SS is ~0.05 (the absolute value), which is much lower than that of DPD and ECAP (1 pass & 3 pass) 316L SS (0.10–0.15) [21,49] (Table 1). The lower absolute value of b indicates higher resistance to strain localization and fatigue crack initiation and propagation [52]. This is consistent with our observations of the higher fatigue resistance to interface cracking initiation and propagation in nanotwin strengthened 316L SS.

Fig. 10b shows the comparison of fatigue properties of nanotwin strengthened 316L SS and other second phase reinforced steels [53–55]. The stress amplitude is normalized by ultimate tensile strength to cancel out tensile strength effect. The normalized fatigue strength of nanotwin strengthened 316L SS is higher than that of most conventional second phase reinforced steels, such as ferrite-martensite (F-M) and ferrite-pearlite (F–P) and ferrite-bainite-martensite (F–B-M) alloys [53–55]. As shown in Table 1, the nanotwin strengthened 316L SS also shows a lower fatigue strength exponent (absolute value of b) in comparison with some second phase reinforced steels. Such better fatigue properties of the nanotwinned SS is attributed to its fatigue deformation and damage mechanisms. The good deformation compatibility between nanotwinned and SRX grains suppressed the strain localization and crack initiation at the nanotwinned/SRX grain interfaces. Also, the high strength and stability of nanotwins effectively retarded fatigue crack initiation. Specifically, twin/matrix lamellae can effectively

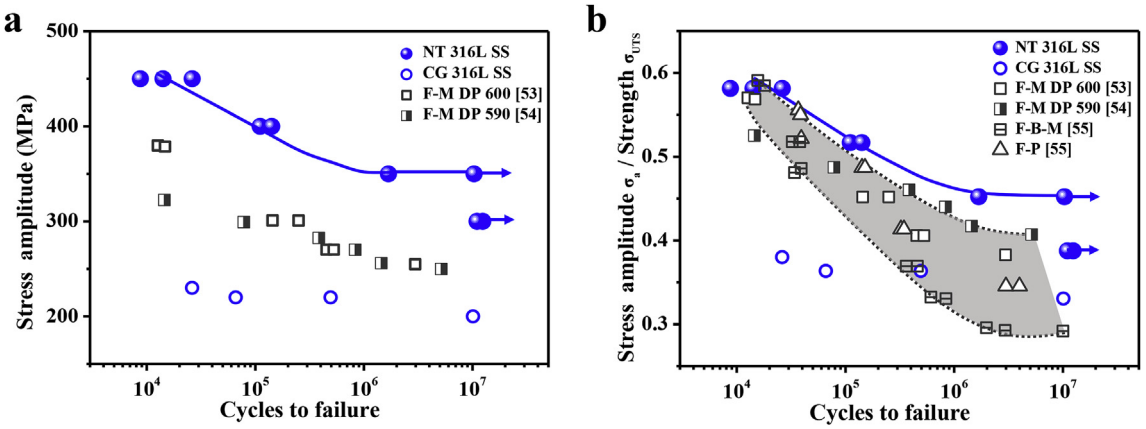

Fig. 10. (a) Stress amplitude-number of cycles (S-N) curves of nanotwin strengthened (NT) and coarse grained (CG) 316L samples. (b) The stress amplitudes of the steels in (a) are normalized by their ultimate tensile strength (σ_{UTS}), respectively. S-N curves of ferrite-martensite dual-phase steels (F-M DP 600 [53] and F-M DP 590 [54]), ferrite-pearlite (F-P) steel [55] and ferrite-bainite-martensite (F-B-M) multiphase steel [55] were included for comparison.

Table 1
Tensile and fatigue properties of nanotwin strengthened (NT) 316L SS, in comparison with those of coarse grained (CG), DPD, equal channel angular pressing (ECAP) treated 316L SS samples and dual-phase (DP)/multiphase steels, including ferrite-martensite (F-M), ferrite-bainite-martensite (F-B-M) and ferrite-pearlite (F-P) steels.

	Samples	σ_{UTS} (MPa)	σ_f (MPa)	σ_f/σ_{UTS}	b
316L SS	NT 316L SS	774	350	0.45	−0.05
	CG 316L SS	605	200	0.33	−0.02
	CG 316L SS [56]	588	220	0.37	−0.05
	DPD 316 L SS [21]	1215	425	0.35	−0.10
	1Pass-ECAP 316L SS [49]	900 ± 20	360 ± 5	0.40	−0.15
	3Pass-ECAP 316L SS [49]	1340 ± 20	570 ± 10	0.40	−0.11
Dual-phase/multiphase steels	F-M DP 600 [53]	666	255	0.38	−0.09
	F–B-M [55]	1370	400	0.29	−0.14
	F–P [55]	970	340	0.35	−0.10

suppress crack propagation by deflecting cracks in terms of kinks and branches [15,21,24–26,42,43,57,58]. Therefore, the partially recrystallized nanotwin strengthened 316L SS studied here exhibited an enhanced fatigue damage resistance and thus improved fatigue properties in comparison with conventional DP steels.

5. Conclusions

We investigated the fatigue damage behavior and cyclic deformation mechanism of nanotwin strengthened 316L SS consisting of hard nanotwinned grains and a soft partially recrystallized matrix. Over half of the cracks (57% in number fraction) are found in SRX grains (about 45% in SRX grains close to nanotwins) rather than at interfaces (11%). The nanotwinned/SRX grain interface crack susceptibility significantly decreases in comparison with conventional phase boundaries where most cracks initiate and propagate in hard phase reinforced materials. Such high crack resistance of nanotwinned/SRX grain interface is closely related to the cyclic deformation mechanism.

At small cumulative cyclic strains (below 4000 cycles at $\sigma_a = 450$ MPa), strain localization and strain gradient effects around the nanotwinned/SRX grain interfaces are modest in comparison with two phase materials with higher mechanical contrast among the phases. The nanotwinned grains can sustain a certain amount of cyclic strains by dislocation slip and storage (specifically the well-ordered threading dislocations slip confined within the twin lamellae) and thus deform compatibly with SRX matrix. At large cumulative cyclic strains (over 4000 cycles at $\sigma_a = 450$ MPa), inhomogeneous cyclic deformation with a moderate strain gradient occurred in the surrounding SRX grains as a function of distance from the interface. Strain localization initiated in nanotwinned grains in the form of shear banding, which resulted in more severe deformation of SRX grains close to interfaces. Nanotwins were stable without obviously de-twinning and coarsening during cyclic deformation, thereby suppressing crack propagation.

The nanotwin strengthened 316L SS exhibited an improved fatigue ratio of 0.45 and fatigue limit of ~350 MPa, superior to that of conventional second phase reinforced steels with comparable tensile strength. Nanotwin strengthening may thus offer a novel approach to design high fatigue damage resistance engineering alloys.

Acknowledgements

Financial support from the National Natural Science Foundation of China (Grant No. 51501191, 51771196and U1730140), National Key R&D Program of China (Grant No. 2017YFA0204401 and 2017YFA0204402), the Key Research Program of Frontier Science, Chinese Academy of Sciences and the Alexander von Humboldt Foundation is acknowledged. We thank L. Lu for fruitful discussions.

References

[1] R.G. Davies, Influence of martensite composition and content on the properties of dual phase steels, Metall. Trans. A 9 (1978) 671–679.
[2] M.S. Rashid, Dual phase steels, Annu. Rev. Mater. Sci. 11 (1981) 245–266.
[3] A. Bag, K.K. Ray, E.S. Dwarakadasa, Influence of martensite content and morphology on the toughness and fatigue behavior of high-martensite dual-phase steels, Metall. Mater. Trans. 32 (2001) 2207–2217.
[4] M. Calcagnotto, Y. Adachi, D. Ponge, D. Raabe, Deformation and fracture mechanisms in fine- and ultrafine-grained ferrite/martensite dual-phase steels and the effect of aging, Acta Mater. 59 (2011) 658–670.
[5] Z.G. Wang, G.N. Wang, W. K, H.C. He, Influence of the martensite content on the fatigue behavior of a dual-phase steel, Mater. Sci. Eng., A 91 (1987) 39–44.
[6] M. Okayasu, K. Sato, M. Mizuno, D.Y. Hwang, D.H. Shin, Fatigue properties of ultra-fine grained dual phase ferrite/martensite low carbon steel, Int. J. Fatig. 30 (2008) 1358–1365.
[7] S. Majumdar, S. Roy, K.K. Ray, Fatigue performance of dual-phase steels for automotive wheel application, Fatig. Fract. Eng. Mater. Struct. 40 (2017) 315–332.
[8] Q. Lai, O. Bouaziz, M. Gouné, L. Brassart, M. Verdier, G. Parry, A. Perlade, Y. Bréchet, T. Pardoen, Damage and fracture of dual-phase steels: influence of martensite volume fraction, Mater. Sci. Eng., A 646 (2015) 322–331.
[9] M.F. Ashby, The deformation of plastically non-homogeneous materials, Philos. Mag. A 21 (1970) 399–424.
[10] J. Kadkhodapour, S. Schmauder, D. Raabe, S. Ziaei-Rad, U. Weber, M. Calcagnotto, Experimental and numerical study on geometrically necessary dislocations and non-homogeneous mechanical properties of the ferrite phase in dual phase steels, Acta Mater. 59 (2011) 4387–4394.
[11] B. Anbarlooie, H. Hosseini-Toudeshky, J. Kadkhodapour, High cycle fatigue micromechanical behavior of dual phase steel: damage initiation, propagation and final failure, Mech. Mater. 106 (2017) 8–19.
[12] C.C. Tasan, M. Diehl, D. Yan, C. Zambaldi, P. Shanthraj, F. Roters, D. Raabe, Integrated experimental–simulation analysis of stress and strain partitioning in multiphase alloys, Acta Mater. 81 (2014) 386–400.
[13] D. Yan, C.C. Tasan, D. Raabe, High resolution in situ mapping of microstrain and microstructure evolution reveals damage resistance criteria in dual phase steels, Acta Mater. 96 (2015) 399–409.
[14] D. Raabe, S. Sandlöbes, J. Millán, D. Ponge, H. Assadi, M. Herbig, P.-P. Choi, Segregation engineering enables nanoscale martensite to austenite phase transformation at grain boundaries: a pathway to ductile martensite, Acta Mater. 61 (2013) 6132–6152.
[15] M.M. Wang, C.C. Tasan, D. Ponge, A.C. Dippel, D. Raabe, Nanolaminate transformation-induced plasticity–twinning-induced plasticity steel with dynamic strain partitioning and enhanced damage resistance, Acta Mater. 85 (2015) 216–228.
[16] M. Koyama, Z. Zhang, M.M. Wang, D. Ponge, D. Raabe, K. Tsuzaki, H. Noguchi, C.C. Tasan, Bone-like crack resistance in hierarchical metastable nanolaminate steels, Science 355 (2017) 1055–1057.
[17] K. Lu, F.K. Yan, H.T. Wang, N.R. Tao, Strengthening austenitic steels by using nanotwinned austenitic grains, Scripta Mater. 66 (2012) 878–883.
[18] F.K. Yan, N.R. Tao, F. Archie, I. Gutierrez-Urrutia, D. Raabe, K. Lu, Deformation mechanisms in an austenitic single-phase duplex microstructured steel with nanotwinned grains, Acta Mater. 81 (2014) 487–500.
[19] F.K. Yan, G.Z. Liu, N.R. Tao, K. Lu, Strength and ductility of 316L austenitic stainless steel strengthened by nano-scale twin bundles, Acta Mater. 60 (2012) 1059–1071.
[20] K. Lu, L. Lu, S. Suresh, Strengthening materials by engineering coherent internal boundaries at the nanoscale, Science 324 (2009) 349–352.
[21] Q. Li, F.K. Yan, N.R. Tao, Enhanced fatigue damage resistance of nanotwinned austenitic grains in a nanotwinned stainless steel, Scripta Mater. 136 (2017) 59–63.

[22] Q.S. Pan, H.F. Zhou, Q.H. Lu, H.J. Gao, L. Lu, History-independent cyclic response of nanotwinned metals, Nature 551 (2017) 214–217.
[23] Q.S. Pan, Q.H. Lu, L. Lu, Fatigue behavior of columnar-grained Cu with preferentially oriented nanoscale twins, Acta Mater. 61 (2013) 1383–1393.
[24] P.B. Chowdhury, H. Sehitoglu, R.G. Rateick, H.J. Maier, Modeling fatigue crack growth resistance of nanocrystalline alloys, Acta Mater. 61 (2013) 2531–2547.
[25] P.B. Chowdhury, H. Sehitoglu, R.G. Rateick, Recent advances in modeling fatigue cracks at microscale in the presence of high density coherent twin interfaces, Curr. Opin. Solid State Mater. Sci. 20 (2016) 140–150.
[26] L.L. Li, Z.J. Zhang, P. Zhang, J.B. Yang, Z.F. Zhang, Distinct fatigue cracking modes of grain boundaries with coplanar slip systems, Acta Mater. 120 (2016) 120–129.
[27] F.K. Yan, Q. Li, N.R. Tao, Anisotropic strengthening of nanotwinned austenitic grains in a nanotwinned stainless steel, Scripta Mater. 142 (2018) 15–19.
[28] M. Calcagnotto, D. Ponge, E. Demir, D. Raabe, Orientation gradients and geometrically necessary dislocations in ultrafine grained dual-phase steels studied by 2D and 3D EBSD, Mater. Sci. Eng., A 527 (2010) 2738–2746.
[29] S.I. Wright, M.M. Nowell, D.P. Field, A review of strain analysis using electron backscatter diffraction, Microsc. Microanal. 17 (2011) 316–329.
[30] F. Archie, S. Zaefferer, On variant selection at the prior austenite grain boundaries in lath martensite and relevant micro-mechanical implications, Mater. Sci. Eng., A 731 (2018) 539–550.
[31] F.K. Yan, N.R. Tao, K. Lu, Tensile ductility of nanotwinned austenitic grains in an austenitic steel, Scripta Mater. 84–85 (2014) 31–34.
[32] J. Man, K. Obrtlík, C. Blochwitz, J. Polák, Atomic force microscopy of surface relief in individual grains of fatigued 316L austenitic stainless steel, Acta Mater. 50 (2002) 3767–3780.
[33] M. Mineur, P. Villechaise, J. Mendez, Influence of the crystalline texture on the fatigue behavior of 316L austenitic stainless steel, Mater. Sci. Eng., A 286 (2000) 257–268.
[34] C.W. Shao, P. Zhang, R. Liu, Z.J. Zhang, J.C. Pang, Z.F. Zhang, Low-cycle and extremely-low-cycle fatigue behaviors of high-Mn austenitic TRIP/TWIP alloys: property evaluation, damage mechanisms and life prediction, Acta Mater. 103 (2016) 781–795.
[35] C. Laird, P. Charsley, H. Mughrabi, Low energy dislocation structures produced by cyclic deformation, Mater. Sci. Eng., A 81 (1986) 433–450.
[36] Y.F. Li, C. Laird, Cyclic response and dislocation structures of AISI 316L stainless steel. Part 2: polycrystals fatigued at intermediate strain amplitude, Mater. Sci. Eng., A 186 (1994) 87–103.
[37] J.L. Zhang, D. Raabe, C.C. Tasan, Designing duplex, ultrafine-grained Fe-Mn-Al-C steels by tuning phase transformation and recrystallization kinetics, Acta Mater. 141 (2017) 374–387.
[38] C.S. Hong, N.R. Tao, X. Huang, K. Lu, Nucleation and thickening of shear bands in nano-scale twin/matrix lamellae of a Cu–Al alloy processed by dynamic plastic deformation, Acta Mater. 58 (2010) 3103–3116.
[39] P. Zhou, Z.Y. Liang, R.D. Liu, M.X. Huang, Evolution of dislocations and twins in a strong and ductile nanotwinned steel, Acta Mater. 111 (2016) 96–107.
[40] C.J. Shute, B.D. Myers, S. Xie, S.-Y. Li, T.W. Barbee Jr., A.M. Hodge, J.R. Weertman, Detwinning, damage and crack initiation during cyclic loading of Cu samples containing aligned nanotwins, Acta Mater. 59 (2011) 4569–4577.
[41] N.M. Heckman, M.F. Berwind, C. Eberl, A.M. Hodge, Microstructural deformation in fatigued nanotwinned copper alloys, Acta Mater. 144 (2018) 138–144.
[42] B.G. Yoo, S.T. Boles, Y. Liu, X. Zhang, R. Schwaiger, C. Eberl, O. Kraft, Quantitative damage and detwinning analysis of nanotwinned copper foil under cyclic loading, Acta Mater. 81 (2014) 184–193.
[43] X.Y. Li, M. Dao, C. Eberl, A.M. Hodge, H.J. Gao, Fracture, fatigue, and creep of nanotwinned metals, MRS Bull. 41 (2016) 298–304.
[44] X.Y. Li, Y.J. Wei, L. Lu, K. Lu, H.J. Gao, Dislocation nucleation governed softening and maximum strength in nanotwinned metals, Nature 464 (2010) 877–880.
[45] L.L. Zhu, H.H. Ruan, X.Y. Li, M. Dao, H.J. Gao, J. Lu, Modeling grain size dependent optimal twin spacing for achieving ultimate high strength and related high ductility in nanotwinned metals, Acta Mater. 59 (2011) 5544–5557.
[46] J. Wang, N. Li, O. Anderoglu, X. Zhang, A. Misra, J.Y. Huang, J.P. Hirth, Detwinning mechanisms for growth twins in face-centered cubic metals, Acta Mater. 58 (2010) 2262–2270.
[47] V. Borovikov, M.I. Mendelev, A.H. King, R. LeSar, Effect of stacking fault energy on mechanism of plastic deformation in nanotwinned FCC metals, Model. Simulat. Mater. Sci. Eng. 23 (2015), 055003.
[48] T. Roland, D. Retraint, K. Lu, J. Lu, Fatigue life improvement through surface nanostructuring of stainless steel by means of surface mechanical attrition treatment, Scripta Mater. 54 (2006) 1949–1954.
[49] H. Ueno, K. Kakihata, Y. Kaneko, S. Hashimoto, A. Vinogradov, Enhanced fatigue properties of nanostructured austenitic SUS 316L stainless steel, Acta Mater. 59 (2011) 7060–7069.
[50] H.W. Huang, Z.B. Wang, J. Lu, K. Lu, Fatigue behaviors of AISI 316L stainless steel with a gradient nanostructured surface layer, Acta Mater. 87 (2015) 150–160.
[51] T. Hanlon, Y.-N. Kwon, S. Suresh, Grain size effects on the fatigue response of nanocrystalline metals, Scripta Mater. 49 (2003) 675–680.
[52] R.H. Li, Z.J. Zhang, P. Zhang, Z.F. Zhang, Improved fatigue properties of ultrafine-grained copper under cyclic torsion loading, Acta Mater. 61 (2013) 5857–5868.
[53] I.H. Onn, N. Ahmad, M.N. Tamin, Fatigue characteristics of dual-phase steel sheets, J. Mech. Sci. Technol. 29 (2015) 51–57.
[54] S.K. Giri, D. Bhattacharjee, Fatigue behavior of thin sheets of DP590 dual-phase steel, J. Mater. Eng. Perform. 21 (2012) 988–994.
[55] S. Sankaran, V.S. Sarma, K.A. Padmanabhan, G. Jaeger, A. Koethe, High cycle fatigue behaviour of a multiphase microalloyed medium carbon steel: a comparison between ferrite–pearlite and tempered martensite microstructures, Mater. Sci. Eng., A 362 (2003) 249–256.
[56] J.P. Strizak, H. Tian, P.K. Liaw, L.K. Mansur, Fatigue properties of type 316LN stainless steel in air and mercury, J. Nucl. Mater. 343 (2005) 134–144.
[57] S. Suresh, Fatigue crack deflection and fracture surface contact: micro-mechanical models, Metall. Trans. A 16 (1985) 249–260.
[58] A. Sing, L. Tang, M. Dao, L. Lu, S. Suresh, Fracture toughness and fatigue crack growth characteristics of nanotwinned copper, Acta Mater. 59 (2011) 2437–2446.